# Electrodeposition of Metals in Catalyst Synthesis: The Case of Platinum Monolayer Electrocatalysts

*by Miomir B. Vukmirovic, Stoyan T. Bliznakov, Kotaro Sasaki, Jia X. Wang, and Radoslav R. Adzic*

The concern about energy sources, their availability, and related environmental effects, is at an all time high. Proton Exchange Membrane Fuel Cells (PEMFCs)—with an efficiency higher than that of internal combustion engines, light weight, low operating temperature, and fast-start-up capability—are strong candidates for automotive applications.[1] Transportation applications could be especially important in shaping up the new energy economy since they may entail a substantial decrease in the adverse environmental effects linked to the use of fossil fuels and prolong their availability. The largest portion of the cost of PEMFCs reflects the large amount of Pt needed in the cathode's catalytic layer due to the low catalytic activity of Pt for the oxygen reduction reaction (ORR). Recently, considerable advances have been made in fuel cell electrocatalysis[2-5] yielding improved electrocatalysts, and increasing our understanding of the kinetics of the ORR in combination with significant advances in theoretical treatments.[6-8] Some of these studies involved: (1.) alloying Pt to synthesize bi-metallic catalysts,[4] (2.) core-shell nanoparticles catalysts,[9] (3.) the role of size, structure, and shape of nanoparticles,[10] and (4.) de-alloying of bimetallic alloys.[11] However, a complete understanding of the ORR kinetics on Pt, the best single element catalyst, and of its low efficiency, is yet to be achieved. These problems, compounded with the high Pt content in current cathode catalysts, and with their gradual loss of performance under operating conditions, still hamper commercialization of fuel cells.[12]

In order to minimize the amount of noble metal electrocatalysts and maximize their utilization, while achieving high catalytic activity, numerous synthetic approaches have been attempted. The electrocatalysts were prepared using vacuum deposition methods,[13] wet chemistry methods,[14] or electrodeposition techniques.[15] Electrodeposition in particular has several attractive features with respect to the application in catalyst synthesis such as simplicity of operation and ease of control of the deposition conditions. In this article we describe the application of metal electrodeposition in the synthesis of a new type of electrocatalysts comprising a Pt monolayer ($Pt_{ML}$) on metal or alloy nanoparticles.

The concept of $Pt_{ML}$ electrocatalysts offers a possible solution to the impasse caused by a slow ORR kinetics and the consequent large Pt content of conventional electrocatalysts. A $Pt_{ML}$ shell on a nanoparticle substrate core ensures that every Pt atom is available for catalytic activity; in other words, a $Pt_{ML}$ achieves the ultimate reduction in Pt loading and complete Pt utilization. Also, through geometric and electronic interaction with the substrate a $Pt_{ML}$ can change its electronic properties and be more active and durable than pure-Pt electrocatalysts.

## Synthesis of $Pt_{ML}$ Electrocatalysts

Synthesis of $Pt_{ML}$ electrocatalysts was accomplished by placing a monolayer of Pt atoms on metal nanoparticles using galvanic displacement of an underpotentially deposited (UPD) Cu monolayer by a Pt monolayer.[16] Underpotential deposition[17, 18] describes the formation of a submonolayer or monolayer of a metal on a foreign metallic substrate at potentials positive to the reversible Nernst potential, that is, before bulk deposition can occur.

The experimental setup for $Pt_{ML}$ deposition (Fig. 1) consists of two cells and a secondary compartment with sliding cover. One cell is a regular electrochemical (EC) cell containing a deareated solution for Cu UPD (50 mM $CuSO_4$ + 50 mM $H_2SO_4$). The other cell contains a deareated Pt solution (1 mM $K_2PtCl_4$ + 50 mM $H_2SO_4$). These two cells are connected with a secondary compartment made of Teflon and glass. The two cells and secondary compartment comprise a closed system. The volume above the solutions and inside the secondary compartment is filled with inert ($O_2$ free) atmosphere (Ar or $N_2$).

The deposition procedure involves two steps. First, the Cu UPD layer is formed in an EC cell. Then, after removing potential control the electrode with the Cu UPD layer on it is transferred to a cell containing the Pt solution. Pt replaces the underpotentially deposited Cu by a simple redox exchange. In order to prevent the oxidation of Cu adatoms in contact with $O_2$[19], the transfer of the electrode from one cell to the other must be done in $O_2$ free atmosphere. This is accomplished by moving the electrode via a secondary compartment

*(continued on next page)*

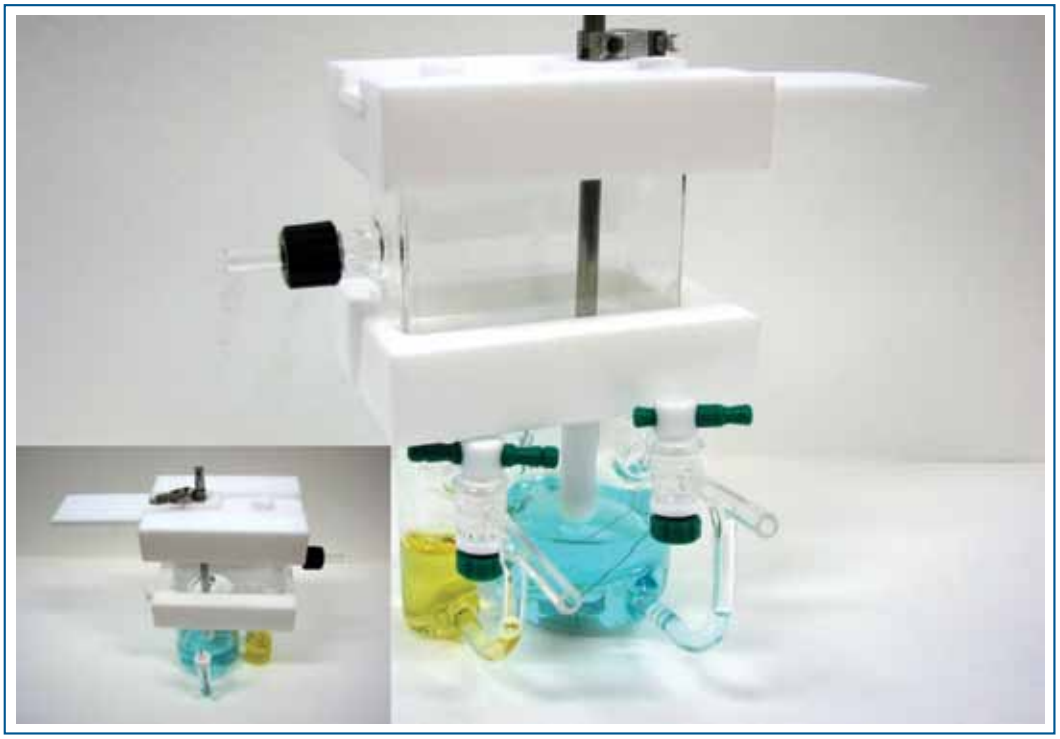

**Fig. 1.** *Cells and setup for $Pt_{ML}$ deposition by displacement of Cu UPD monolayer.*

*(continued from previous page)*

which is filled with inert atmosphere. The exchange reaction is influenced by the choice of UPD metal ($Cu^{2+}$ vs. $Pb^{2+}$), its valency ($Cu^{2+}$ vs. $Tl^{+}$), valency of deposited metal ($Pt^{2+}$ vs. $Pt^{4+}$) and presence of anions and oxidative agents such as oxygen and hydrogen ions.[19-25] A schematic diagram of the entire process is shown in Fig. 2.

As an example of the results obtained for a $Pt_{ML}$ deposition on single crystal electrodes we show the data for a Rh(111) surface.[26] Figure 3 shows the typical voltammetry curve with two peaks for the UPD of Cu on a Rh(111) surface. The charge associated with these peaks is 540 μC/cm², which is close to 524 μC/cm², needed for depositing a pseudomorphic monolayer of Cu on an ideal Rh(111) surface. The most negative peak is very close to the bulk deposition of Cu, which imposes careful control of the Cu UPD process to avoid deposition of more than one monolayer of Cu. This is critical since the amount of deposited Pt corresponds to the UPD Cu coverage. The dashed line shows the curve for a Rh(111) surface in the absence of Cu ions in solution. Figure 4 is the *in situ* scanning tunneling microscopy (STM) image of the $Pt_{ML}$ deposited using galvanic displacement of a Cu monolayer on a Rh(111) surface obtained at open circuit potential in 0.1M $HClO_4$ solution. The deposit consists of two-dimensional interconnected Pt islands. Due to the small difference between the Pt and Rh lattice constants, these islands are expected to be epitaxial with the Rh(111) substrate. There are a certain number of holes between the islands, and also a few sites with Pt atoms in the second layer.

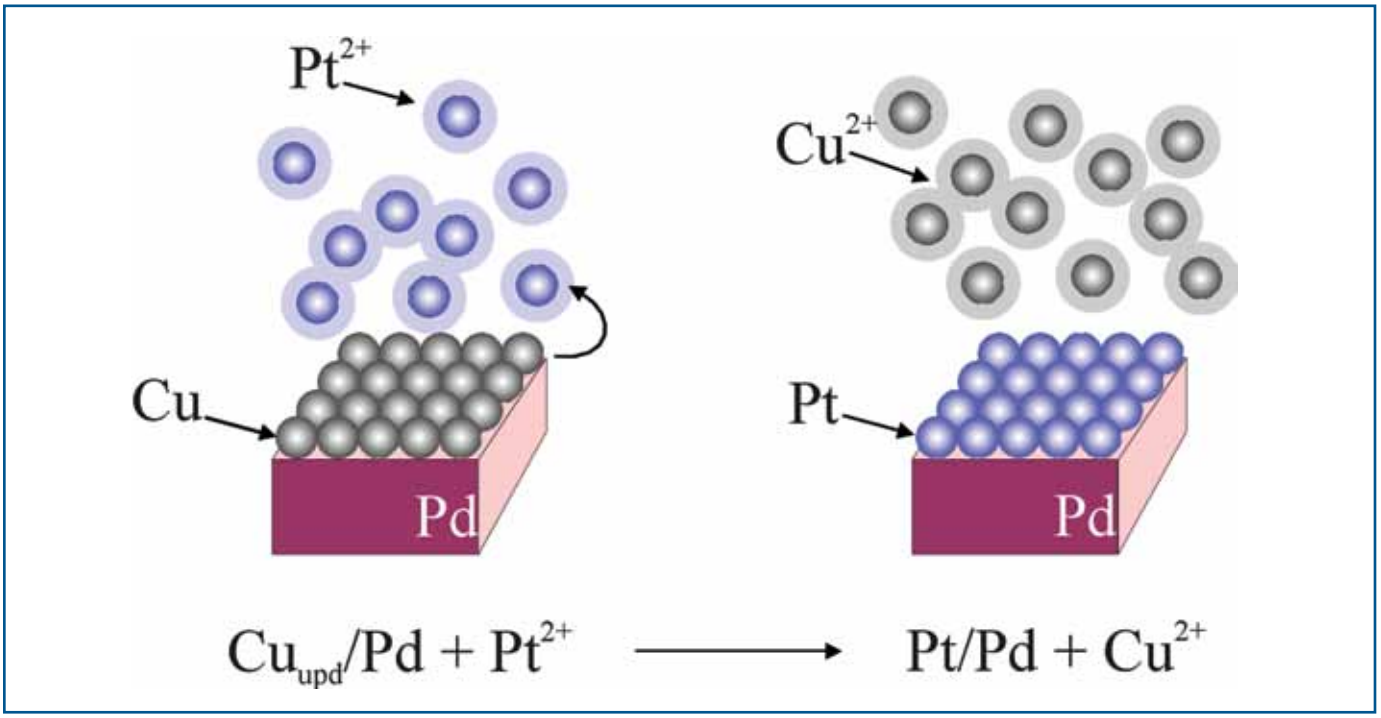


**Fig. 2.** *Schematics of the galvanic displacement of a Cu UPD monolayer by Pt. Blue and gray balls represent Pt and Cu atoms, respectively. The clouds around balls indicate ions.*

## Synthesis of $Pt_{ML}$ by Surface Mediated Growth

To generate Pt shells with controlled morphology and thickness on a Pd core,[10] viz, $Pd_CPt_n$ nanoparticles (with n being the number of Pt layers in the shell on Pd cores) we utilized a Cu UPD mediated electrodeposition method.[27] Figure 5a shows the voltammetry curves for Cu UPD on Pd and Pt nanoparticle catalysts, wherein a full monolayer of Cu is deposited and removed during potential cycles positive of the bulk Cu deposition potential (0.36 V). An irreversible deposition of Pt under diffusion control takes place below its bulk deposition potential (0.67 V) in the solution containing 0.1 mM $K_2PtCl_4$ and 50 mM $Cu^{2+}$. With repeated potential cycles between 0.37 and 0.67 V, the Cu UPD current gradually increases (green curves in Fig. 5b), reflecting the enlargement of the surface area as the size of the core-shell nanoparticles grows by irreversibly deposited Pt. The role of Cu UPD and stripping cycle in this electrodeposition process is to lower the rate of Pt deposition and to enhance surface diffusion of Pt adatoms so that a smooth layer forms.[27, 28] At the end of Pt deposition, a linear potential sweep, up to 1 V, completely removes Cu (Figs. 5a and 5b). The number of potential cycles required to deposit a full monolayer of Pt was determined by comparing the rate of increase in measured surface area with the expected values based on the core particles' average diameter. Estimates of Pt loading obtained from averaged Cu UPD stripping charges measured before and after depositing a monolayer yielded a Pt:Pd mass ratio within 15% of the values obtained from measurements of inductively coupled plasma atomic emission spectroscopy.

The atomic structures and component distributions of the $Pd_CPt_n$ nanoparticles were examined using an aberration-corrected scanning tunneling electron microscope (STEM) equipped with electron-energy-loss spectroscopy (EELS). Figures 6a and 6b show atomically resolved HAADF (High Angle Annular Dark Field)-STEM images for the $Pd_CPt_1$ and $Pd_CPt_4$ samples, respectively. The analysis of the Z-contrast HAADF intensity profiles along the scan lines from the center to the edge, using three-dimensional atomic structural models generated from the observed particles' sizes, shapes, and facets show nearly perfect fits to the data (black lines in Figs. 6c and 6d). Figures 6e and 6f illustrate the projections of the structure models in the STEM image planes, and the arrangements of atoms in the vertical columns along the scan lines. The models obtained from the best fits indicate that all and only the surface atoms are Pt for the $Pd_CPt_1$ sample (Fig. 6e), and the Pt shell is 3- or 4-layers thick for the $Pd_CPt_4$ sample (Fig. 6f), confirming the formation of well-defined Pt shells on Pd metal cores.

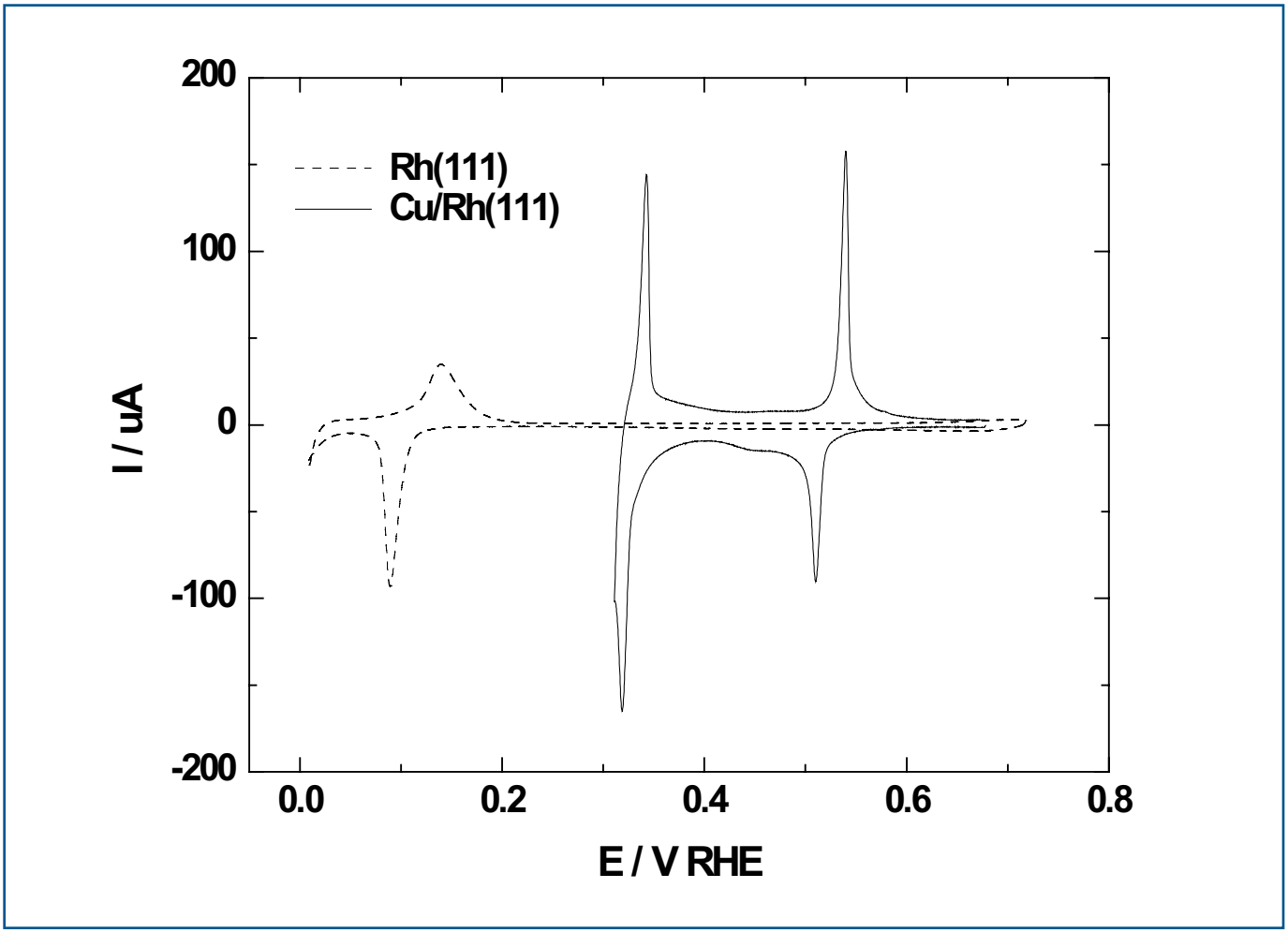


**Fig. 3.** *Voltammetry curves for the underpotential deposition of Cu on a Rh(111) surface (solid line) in 0.05 M $H_2SO_4$ with 0.05 M $Cu^{2+}$, and for a Rh(111) surface in the absence of $Cu^{2+}$ (dashed line); sweep rate 20 mV/s. Reprinted with permission from Ref. 26. (Copyright 2007 American Chemical Society)*

## Electrodeposition of Pd Nanostructures

The ORR activity and stability of $Pt_{ML}$ on Pd nanoparticles supported on carbon ($Pt_{ML}$/Pd/C) electrocatalyst can be improved by changing the shape of Pd nanoparticles. Nanorods/nanowires are chosen instead of nanoparticles to reduce the number of low coordination sites (which are a source of dissolution) in order to improve stability and to increase surface fraction of atoms of the most ORR active facets, thus improving ORR activity as indicated in some recent publications.[10, 29, 30]

The Pd nanostructures were electrochemically deposited from chloride containing solutions (0.1-0.8 mM $PdCl_2$ + 0.1 M NaCl) on thin film high-surface area oxidized carbon ($C_{ox}$), supported on glassy carbon electrode.[31] The surface of oxidized carbon is covered by functional groups that increased the sorption ability of the carbon[32] and improved the nucleation on it.

Figure 7 shows a cyclic voltammetry (CV) curve of Pd electrodeposition on oxidized carbon nanoparticles. There are three pairs of asymmetric cathodic/anodic peaks in the CV curve, observed at potentials more positive than the onset potential for H evolution/oxidation. The first pair of narrow peaks (0.01 - 0.1 V) is attributed to H UPD adsorption/desorption on Pd. The broad pair of peaks (0.1 - 0.15 V) is due to either H UPD or chloride ion adsorption/desorption.[33-35] The most asymmetric couple of cathodic/anodic peaks (0.4 - 0.8 V) is assigned to Pd deposition/dissolution. The negative shift

*(text continued on page 37)*

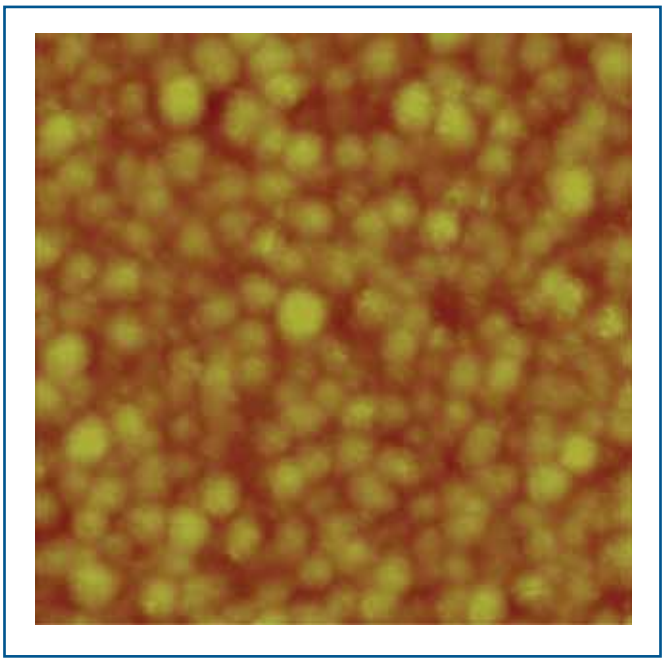

**Fig. 4.** *An* in situ *STM image of $Pt_{ML}$ on a Rh(111) surface obtained at open circuit potential in 0.1 M $HClO_4$ solution. Image size is 47 x 47 nm, Z range 3 nm. Reprinted with permission from Ref. 26. (Copyright 2007 American Chemical Society)*

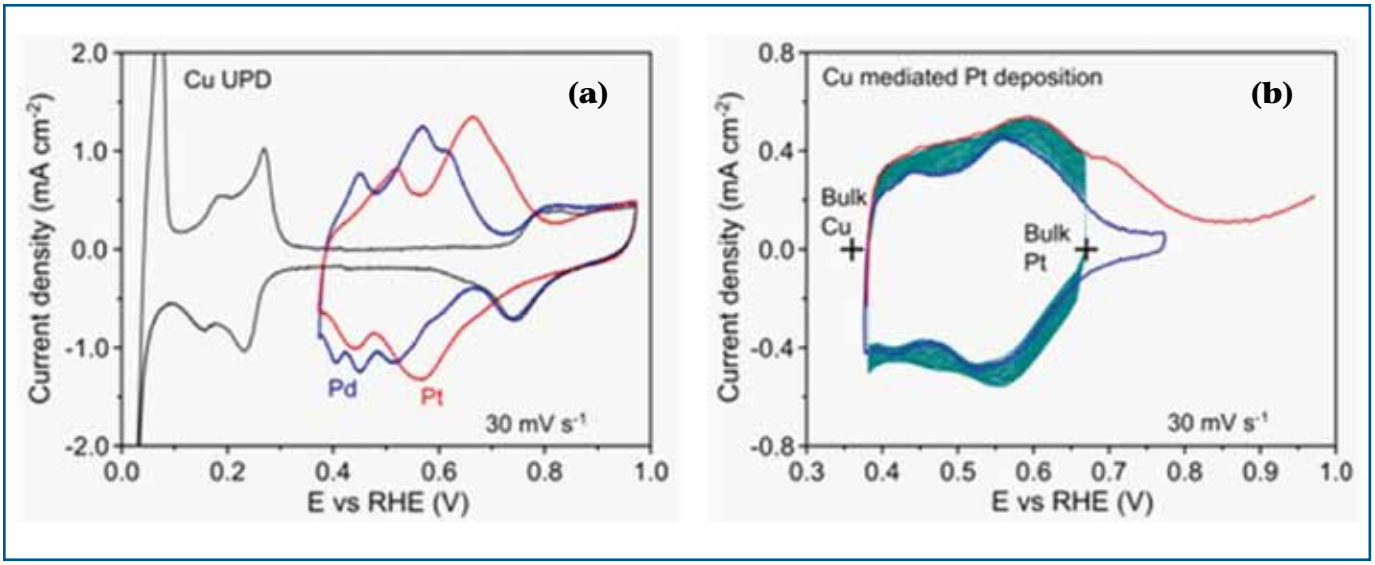


**Fig. 5.** *(a) Voltammetry curves for Cu UPD on Pd (blue) and Pt (red) nanoparticles in Ar-saturated solutions containing 50 mM $H_2SO_4$ and 50 mM $CuSO_4$, together with a baseline voltammetry curve for Pd in a solution without Cu (black). (b) Voltammetry curves before (blue), during (green), and after (red) $Pt_{ML}$ deposition on Pd in the above solution with additional 0.1 mM $K_2PtCl_4$. Reprinted with permission from Ref. 10. (Copyright 2009 American Chemical Society.)*

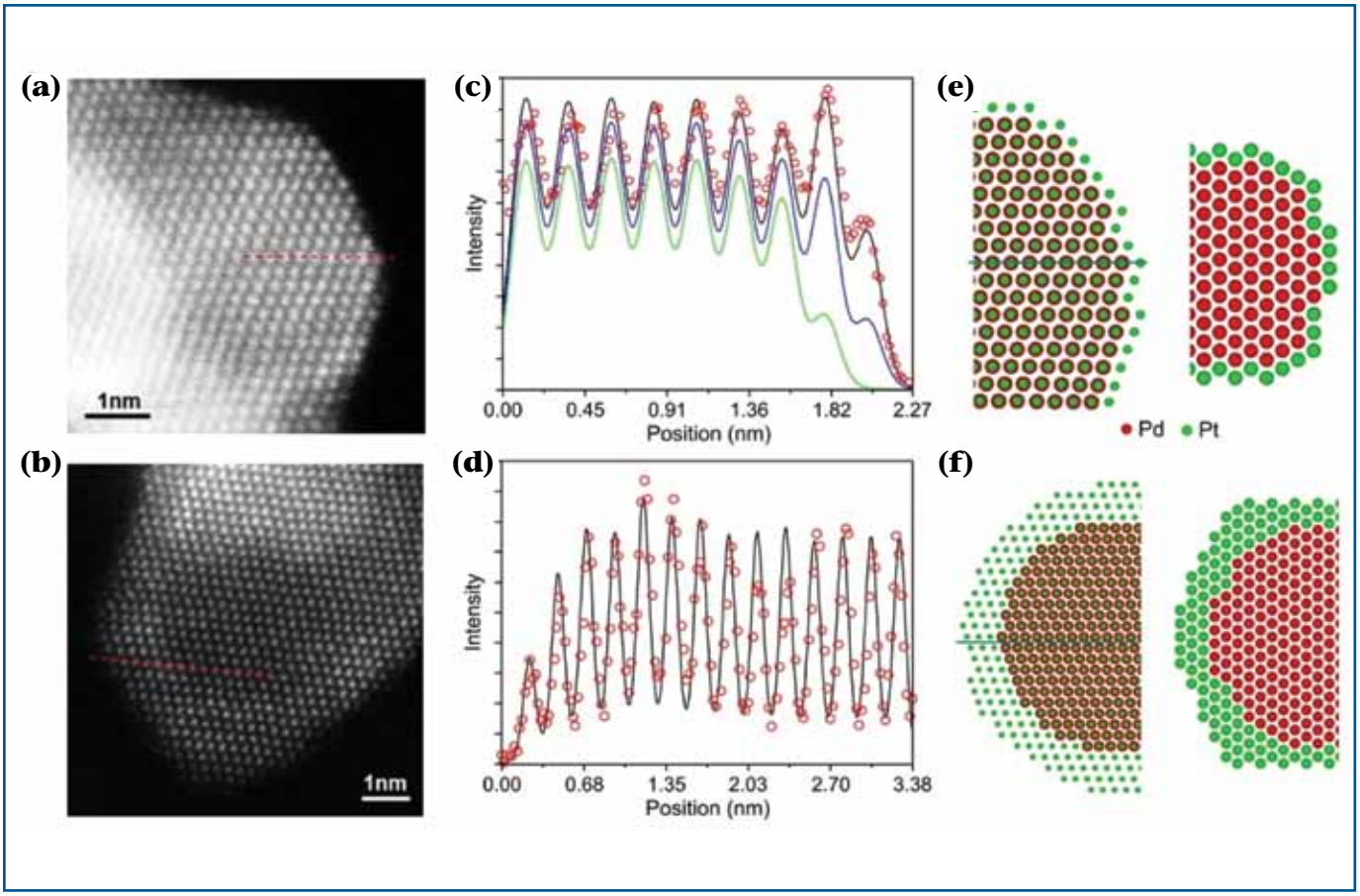


**Fig. 6.** *(a,b) HAADF-STEM images of the Pd(core)-Pt(shell) nanoparticles obtained for the $Pd_cPt_1$ and $Pd_cPt_4$ samples, respectively. We note that the nanoparticles overlap with others at the left side in (a), and at the top side in (b). (c,d) Intensity profiles from the scan lines in (a) and (b) (open circles), and the best fits (black lines), based on the structure models shown in (e) and (f) for Pd particles with 1 and 3-4 Pt surface layers, respectively. The calculations are convoluted with a Gaussian point spread function. Two additional lines in (c) show the calculations made with all the Pt surface atoms being removed (green line), or replaced by Pd (blue line). (e) Projection of the one-Pt-layer core-shell structure model along the [101] direction (left), and the atomic arrangement (right) of the $(1\bar{1}\bar{1})$ plane at the position indicated by the line in the left. (f) Projection of the structure model with 4 Pt layers on the STEM image plane (left) and the arrangements of atoms in the vertical columns along the scan line (right). Reprinted with permission from Ref. 10. (Copyright 2009 American Chemical Society)*

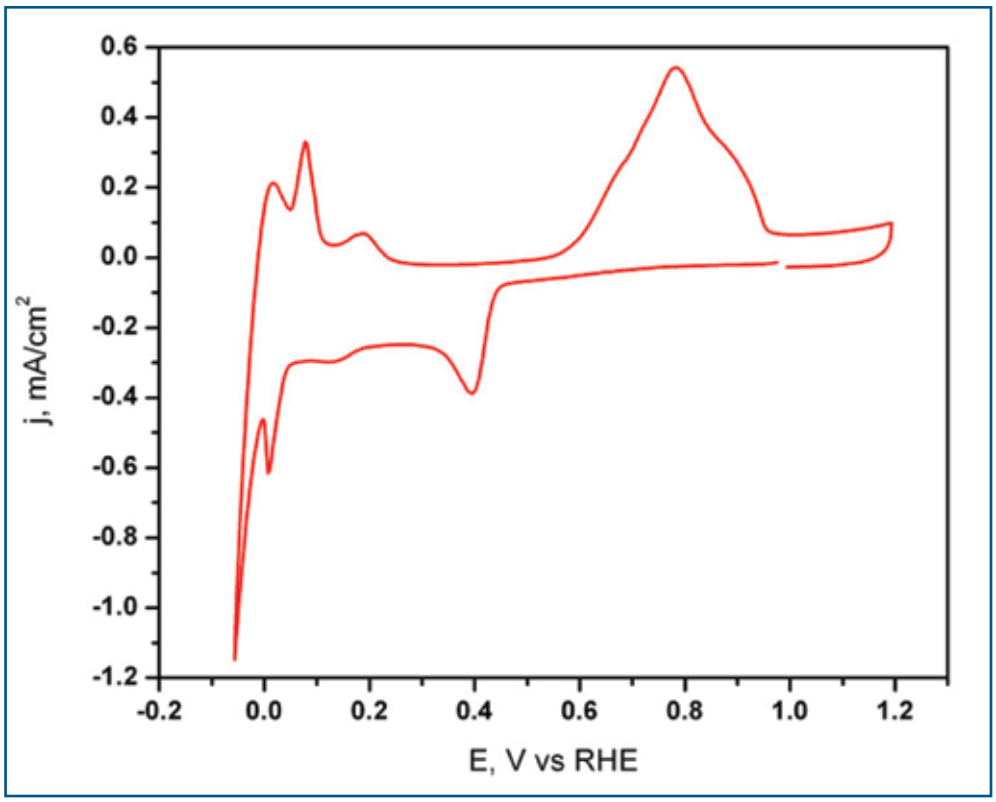


**Fig. 7.** *Cyclic voltammetry curve measured for thin-film oxidized carbon on a GC electrode at scan rate of 10 mV/s in deaerated 0.1 M NaCl +0.8 mM $PdCl_2$ solution.*

*(continued from page 35)*

and asymmetry of these peaks are associated with the strong adsorption of both chloride ions and tetrachloropalladate ($[PdCl_4]^{2-}$) complex existing in the electrolyte on the Pd surface.[36, 37] The negative shift of the onset potential for Pd bulk deposition on $C_{ox}$ is attributed to either a significant overpotential for Pd deposition on carbon or the absence of an ordered adlayer of the $[PdCl_4]^{2-}$ ions on the carbon surface.[33] The potentiostatic current transients (data not shown)[31] suggest an instantaneous two-dimensional nucleation with planar diffusion growth control.[38, 39]

The dependence of the morphology of Pd deposits on the deposition potential is shown in Fig. 8. Generally, it is seen that the shape of the Pd nanostructures is changed from nanoparticles (4-5 nm) to nanorods (aspect ratio of 5-6) and to nanowires (diameter of 3-4 nm and length of 50-60 nm) with increasing deposition overpotential. The mechanism of instantaneous nucleation implies that nuclei are created simultaneously, their number remains constant and their growth rate is the same. Consequently, the change in the growth mechanism could be the only reason for morphology change.

Morphology of Pd nanostructures is determined by the interplay between chloride adsorption and H UPD. With decreasing potential below 0.2 V, the coverage by chloride ions on the cluster's facets decreases, while its coverage by hydrogen atoms increases gradually. The chloride ions adsorbed on the edges of the Pd clusters are those most strongly adsorbed, and they can be desorbed completely at potentials below 0.04 V. Hence, at about 0.05 V, chloride ions are adsorbed only on the edges of the Pd clusters, while UPD-adsorbed hydrogen atoms partially cover the facets. The adsorbed hydrogen on the Pd surface reduces the Pd complex and promotes the layer-by-layer growth of Pd, similarly to the surfactant-mediated two-dimensional growth of Ag on Ag(111) suggested by Brankovic et al.[40] The H UPD layer on the Pd surface enhances the nucleation density[41] as an ideal surfactant, since its high mobility[42] ensures its "floating" on the Pd surface as growth proceeds.[40] So, at this potential Pd predominantly grows in the shape of nanowires because specifically adsorbed chloride-ions block the edges of the clusters causing lateral growth to be hindered. The H UPD coverage decreases with increasing potential, and the surfactant-mediated growth mode is not efficient enough to support the growth of nanowires; thus, the growth mode changes from nanowires to nanorods and finally to nanoparticles.

The high-resolution transmission electron microscopy (HRTEM) images of the samples are presented as insets in Fig. 8. It is seen that all deposited Pd nanostructures are single crystalline. Lattice fringes with interplanar spacing of 0.22 nm, ascribed to (111) planes of the face-centered cubic (fcc) structure of Pd, are clearly seen in the HRTEM images. The

*(continued on next page)*

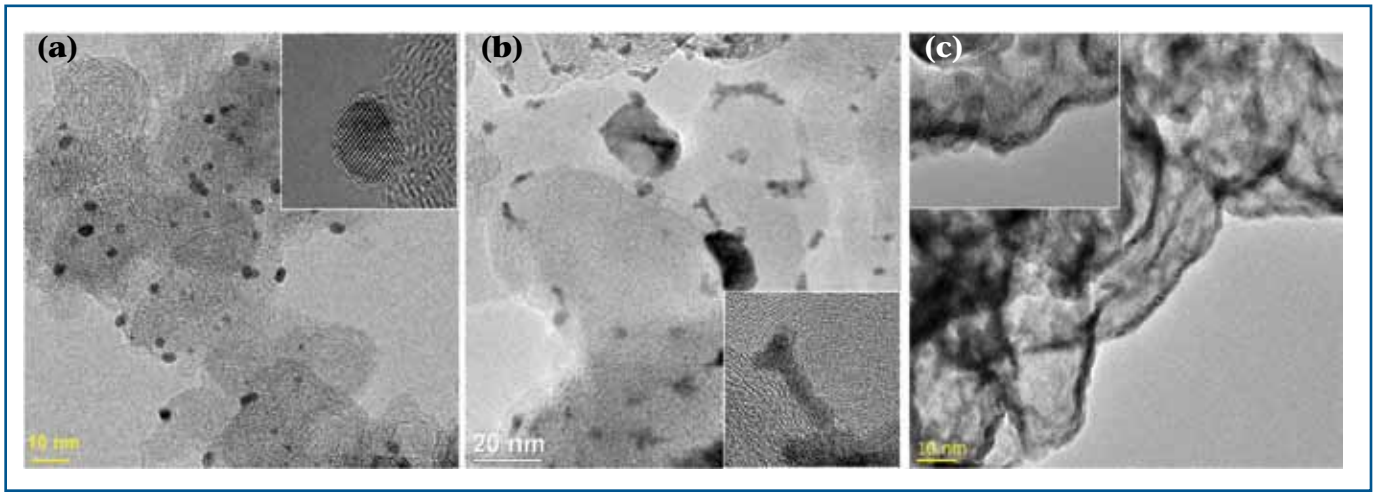


**Fig. 8.** *TEM images of electrodeposited Pd nanoparticles (a), nanorods (b), and nanowires (c). The insets are HRTEM images of the respective nanostructure.*

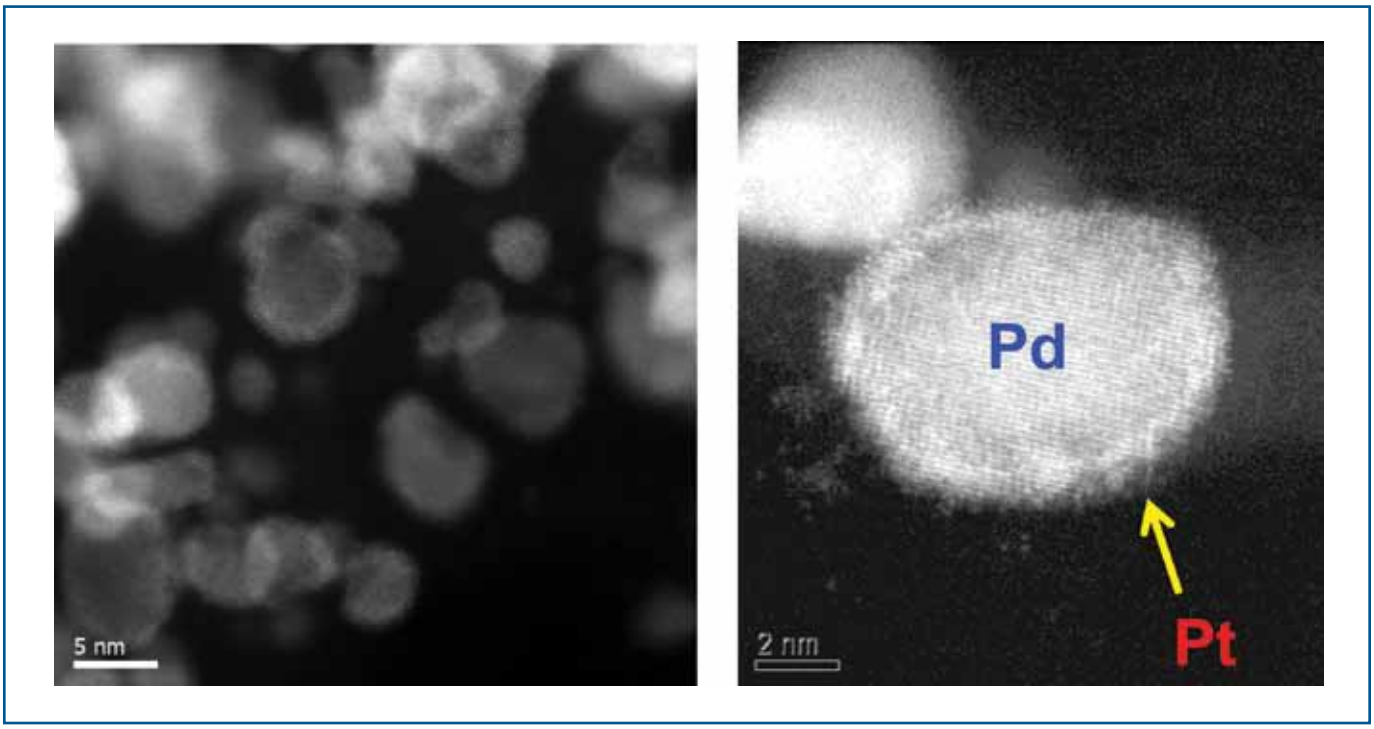


**Fig. 9.** *HAADF images of $Pt_{ML}$/Pd/C electrocatalyst synthesized by scale-up method. Reprinted from Ref. 45. (Copyright 2010 with permission from Elsevier.)*

fast Fourier transform pattern of selected areas from a single nanowire indicated that most of the Pd atoms are ordered in (111) facets. It also confirms that the surface fraction of Pd atoms on the (111) facets is predominant in the sample of interest.

## Example of $Pt_{ML}$ Electrocatalyst

As an example of practical high-activity and high-stability catalysts, the data for $Pt_{ML}$ on Pd nanoparticles supported on carbon ($Pt_{ML}$/Pd/C) are presented.[43] The study of the ORR activity of $Pt_{ML}$ on five single-crystal surfaces showed that $Pt_{ML}$ on Pd(111) had higher ORR activity than Pt(111).[44] The catalyst (2 g) was prepared in a scale up synthesis based on the Cu UPD method.[43, 45]

The morphology and structure of a $Pt_{ML}$/Pd/C electrocatalyst synthesized by the scale-up methodology were examined by HAADF-STEM.[45] The HAADF technique can resolve interfaces/locations between different elements since the image intensity from an element (atomic number Z) follows approximately a $Z^2$ dependence.[46] The Z-contrast images in Fig. 9 show bright shells on relatively darker nanoparticles, which suggest the formation of a core–shell structure, i.e., a Pt (Z = 78) monolayer or bilayer (shell) on a Pd (Z = 46) nanoparticle (core).[45] Figure 10 gives the results of accelerated fuel-cell stability tests of the $Pt_{ML}$/Pd/C electrocatalyst by plotting Pt mass activity as a function of the number of potential cycles.[43] The test involved potential step cycling between 0.7 and 0.9 V (RHE) with a 30 second dwell time at 80°C.[43] After 100,000 cycles, the Pt mass activity was decreased

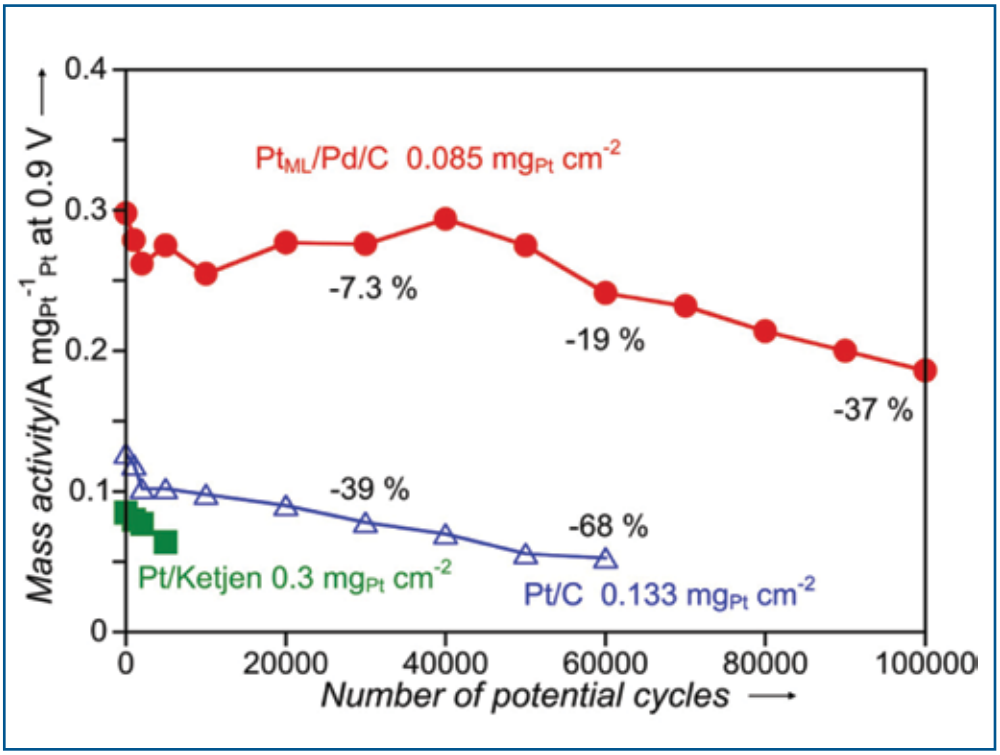


**Fig. 10.** *The Pt mass activity for the ORR as a function of the number of potential cycles during fuel cell testing of the $Pt_{ML}$/Pd/C electrocatalyst. The results with Pt/C and Pt/Ketjen carbon catalysts are shown for comparison. Reproduced with permission from Ref. 43. (Copyright Wiley-VCH Verlag GmbH & Co. KGaA)*

37%, indicating the excellent durability of this electrocatalyst. For comparison, the Pt mass activity of two commercial Pt/C catalysts is about three times smaller than that of the $Pt_{ML}$/Pd/C electrocatalyst. Thus, after 60,000 potential cycles, Pt/C had lost almost 70% of its activity, compared with less than 20% for $Pt_{ML}$/Pd/C; the activity of Pt/Ketjen black carbon had fallen more than 40% after only 10,000 cycles. It is particularly important and informative that at 60,000 cycles, the Pt mass activity of $Pt_{ML}$/Pd/C catalyst increased from the initial threefold to fivefold enhancement over that of Pt/C. This fact clearly illustrates the superior stability of the $Pt_{ML}$/Pd/C.

## Summary

We have described the use of several metal electrodepositon techniques in syntheses of a new class of electrocatalysts comprising a $Pt_{ML}$ on metal or alloy nanoparticles. These electrocatalysts can dramatically reduce the Pt content, while affording enhanced catalytic activity. The galvanic displacement of a Cu UPD monolayer by Pt provides a uniquely convenient way of uniformly depositing a metal monolayer on carbon-supported metal nanoparticles in a surface-limited reaction controllable to a small fraction of a monolayer. This procedure can be extended into the area of thin film metal electrodeposition.[19, 21-23, 47-49] Scale-up of this synthesis method is possible and successfully tested up to 50 grams per batch.[43] The method facilitates growing various nanoparticles architectures with controllable thickness of components in stratified structures. The $Pt_{ML}$ electrocatalysts described above can remove the remaining obstacles in using fuel cells in automotive application. In addition, these findings indicate the broad applicability of the $Pt_{ML}$ catalysts and the possibility of extending this concept to the catalysts based on other noble metals which could prolong the availability of Pt for future use. The environmental benefits resulting from the use of fuel cells in transportation would be an especially important result of the application of $Pt_{ML}$ electrocatalysts.

## Acknowledgments

Work at BNL was supported by U.S. Department of Energy, Divisions of Chemical and Material Sciences, under Contract No. DE-AC02-98CH10886.

## About the Authors

**Radoslav R. Adzic** is a senior chemist and Electrochemistry Group leader in the Chemistry Department at Brookhaven National Laboratory. He is an adjunct professor at Stony Brook University. His research interests include various topics from surface electrochemistry and electrocatalysis, such as structural properties and catalytic effects of metal monolayers, underpotential metal deposition, and electrocatalysts of fuel cell reactions. His recent work is focused on developing platinum monolayer electrocatalysts. He may be reached at adzic@bnl.gov.

**Stoyan T. Bliznakov** is a senior research associate in the Chemistry Department at Brookhaven National Laboratory. His current research interest is in developing advanced Pt monolayer cathode electrocatalysts for the polymer electrolyte membrane fuel cells. Also, he has experience and expertise in developing hydrogen storage materials, negative electrodes for advanced electrochemical power sources, catalysts for polymer electrolyte membrane hydrogen generators, study of the kinetic and thermodynamic aspects of thin film growth, chemical and electrochemical processing of nanoscale materials, development of optimized electrodeposition strategies for improved packaging reliability, and analytical approaches based on surface electrochemistry. He has participated in many projects related to hydrogen storage, hydrogen generation, and fuel cells catalysis funded by U.S. DOE, U.S. NSF, and the European Union. He may be reached at sbliznakov@bnl.gov.

**Kotaro Sasaki** is a chemist in the Chemistry Department at Brookhaven National Laboratory. His research interests include electrocatalysis, direct energy conversion, and nanomaterial characterization by *in situ* X-ray absorption spectroscopy. He has been involved in development of submonolayer/monolayer Pt electrocatalysts for hydrogen and methanol oxidation and oxygen reduction. Recently he also is exploring nanostructured materials for fuel generation (hydrogen and methanol) by water splitting and $CO_2$ reduction. He may be reached at ksasaki@bnl.gov.

**Miomir B. Vukmirovic** is a chemist in the Chemistry Department at Brookhaven National Laboratory. His research advanced fuel cell electrocatalysts for higher activity and improved durability, and for lower cost through reduced Pt loading. His research examines both single crystal model systems for fundamental understanding and structured nanoparticle electrocatalysts for applications. His primary focus has been on the development of Pt monolayer core-shell electrocatalysts for the cathode (oxygen reduction reaction). He may be reached at miomir@bnl.gov.

**Jia X. Wang** is a chemist in the Chemistry Department at Brookhaven National Laboratory. Her research interests include surface electrochemistry using *in situ* surface X-ray scattering, electrocatalysis, fuel cells, and nano-catalyst syntheses. Recently, her work focuses on designing and synthesizing core-shell nanoparticles at the atomic level for electrocatalytic applications. She may be reached at jia@bnl.gov.

## References

1. http:/www1.eere.energy.gov/hydrogenandfuelcells/mypp/
2. H. A. Gasteiger, S. S. Kocha, B. Sompalli, and F. T. Wagner, *Appl. Catal. B*, **56**, 9 (2005).
3. R. R. Adzic, J. Zhang, K. Sasaki, M. B. Vukmirovic, M. Shao, J. X. Wang, A. U. Nilekar, M. Mavrikakis, J. A. Valerio, and F. Uribe, *Top. Catal.*, **46**, 249 (2007).
4. V. R. Stamenkovic, B. S. Mun, M. Arenz, K. J. J. Mayrhofer, C. A. Lucas, G. Wang, P. N. Ross, and N. M. Markovic, *Nat. Mater.*, **6**, 241 (2007).
5. S. Gottesfeld and T. A. Zawodzinski, in *Advances in Electrochemical Science and Engineering*, Vol. 5, R. C. Alkire, H. Gerischer, D. M. Kolb, and C. W. Tobias, Eds., p. 195, Wiley-VCH, New York (1997).
6. B. Hammer and J. K. Nørskov, *Surf. Sci.*, **343**, 211 (1995).
7. B. Hammer and J.K. Nørskov, *Nature*, **376**, 238 (1995).
8. A. U. Nilekar and M. Mavrikakis, *Surf. Sci.*, **602**, L89 (2008).
9. J. Zhang, F. H. B. Lima, M. H. Shao, K. Sasaki, J. X. Wang, J. Hanson, and R. R. Adzic, *J. Phys. Chem. B*, **109**, 22701 (2005).
10. J. X. Wang, H. Inada, L. Wu, Y. Zhu, Y. M. Choi, P. Liu, W-P. Zhou, and R.R. Adzic, *J. Am. Chem. Soc.*, **131**, 17298 (2009).
11. P. Strasser, *Rev. Chem. Eng.*, **25**, 255 (2009).
12. J. Zhang, K. Sasaki, E. Sutter, and R. R. Adzic, *Science*, **315**, 220 (2007).
13. S. Litster and G. McLean, *J. Power Sources*, **130**, 61 (2004).
14. Y. Xia, Y. Xiong, B. Lim, and S. E. Skrabalak, *Angew. Chem. Int. Ed.*, **48**, 60 (2009).
15. H. Kim, N. P. Subramanian, and B. N. Popov, *J. Power Sources*, **138**, 14 (2004).
16. S. R. Brankovic, J. X. Wang, and R. R. Adzic, *Surf. Sci.*, **474**, L173 (2001).
17. D. M. Kolb, in *Advances in Electrochemistry and Electrochemical Engineering*, Vol. 11, H. Gerischer and C. W. Tobias, Eds., p.125, Wiley, New York (1978).
18. E. Budevski, G. Staikov, and W. J. Lorenz, *Electrochemical Phase Formation and Growth*, Wiley-VCH, Weinheim, Germany, (1996).

*(continued on next page)*

# THE ELECTROCHEMICAL SOCIETY MONOGRAPH SERIES

*The following volumes are sponsored by ECS, and published by John Wiley & Sons, Inc. They should be ordered from: ECS, 65 South Main St., Pennington, NJ 08534-2839, USA or www.electrochem.org/dl/bookstore.htm.*

***NEW!***

**Uhlig's Corrosion Handbook (3rd Edition)**
*by R. Winston Revie (2011)*
1288 pages. ISBN 978-0-470-08032-0

**Modern Electroplating (5th Edition)**
*by M. Schlesinger and M. Paunovic (2010)*
736 pages. ISBN 978-0-470-16778-6

**Fuel Cells: Problems and Solutions**
*by V. Bagotsky (2009)*
320 pages. ISBN 978-0-470-23289-7

**Electrochemical Impedance Spectroscopy**
*by M. E. Orazem and B. Tribollet (2008)*
524 pages. ISBN 978-0-470-04140-6

**Fundamentals of Electrochemical Deposition (2nd Edition)**
*by M. Paunovic and M. Schlesinger (2006)*
373 pages. ISBN 978-0-471-71221-3

**Fundamentals of Electrochemistry (2nd Edition)**
*Edited by V. S. Bagotsky (2005)*
722 pages. ISBN 978-0-471-70058-6

**Electrochemical Systems (3rd edition)**
*by John Newman and Karen E. Thomas-Alyea (2004)*
647 pages. ISBN 978-0-471-47756-3

**Modern Electroplating (4th edition)**
*Edited by M. Schlesinger and M. Paunovic (2000)*
888 pages. ISBN 978-0-471-16824-9

**Atmospheric Corrosion**
*by C. Leygraf and T. Graedel (2000)*
3684 pages. ISBN 978-0-471-37219-6

**Uhlig's Corrosion Handbook (2nd edition)**
*by R. Winston Revie (2000). paperback*
1340 pages. ISBN 978-0-471-78494-4

**Semiconductor Wafer Bonding**
*by Q. -Y. Tong and U. Gösele (1999)*
297 pages. ISBN 978-0-471-57481-1

**Corrosion of Stainless Steels (2nd edition)**
*by A. J. Sedriks (1996)*
437 pages. ISBN 978-0-471-00792-0

**Synthetic Diamond: Emerging CVD Science and Technology**
*Edited by K. E. Spear and J. P. Dismukes (1994)*
688 pages. ISBN 978-0-471-53589-8

*ECS Members will receive a discount. All prices subject to change without notice.*

**www.electrochem.org**



*(continued from previous page)*


19. R. Vasilic, N. Vasiljevic, and N. Dimitrov, *J. Electroanal. Chem.*, **580**, 203 (2005).
20. L. T. Viyannalage, R. Vasilic, and N. Dimitrov, *J. Phys. Chem. C*, **111**, 4036 (2007).
21. N. Dimitrov, R. Vasilic, and N. Vasiljevic, *Electrochem. Solid-State Lett.*, **10**, D79 (2007).
22. R. Vasilic and N. Dimitrov, *Electrochem. Solid-State Lett.*, **8**, C173 (2005).
23. R. Vasilic, L. T. Viyannalage, and N. Dimitrov, *J. Electrochem. Soc.*, **153**, C648 (2006).
24. Y. G. Kim, J. Y. Kim, D. Vairavapandian, and J. L. Stickney, *J. Phys. Chem. B*, **110**, 17998 (2006).
25. D. Gokcen, S. E. Bae, and S. R. Brankovic, *J. Electrochem. Soc.*, **157**, D582 (2010).
26. F. H. B. Lima, J. Zhang, M. H. Shao, K. Sasaki, M. B. Vukmirovic, E. A. Ticianelli, and R. R. Adzic, *J. Phys. Chem. C.*, **111**, 404 (2007).
27. K. Sieradzki, S. R. Brankovic, and N. Dimitrov, *Science*, **284**, 138 (1999).
28. J. X. Wang, B. M. Ocko, and R. R. Adzic, *Surf. Sci.*, **540**, 230 (2003).
29. C. Koenigsmann, W. P. Zhou, R. R. Adzic, E. Sutter, and S. S. Wong, *Nano Lett.*, **10**, 2806 (2010).
30. Z. W. Chen, M. Waje, W. Z. Li, and Y. S. Yan, *Angew. Chem. Int. Ed.*, **46**, 4060 (2007).
31. S. S. Bliznakov, M. B. Vukmirovic, E. Sutter, and R. R. Adzic, in preparation.
32. I. I. Salame, T. J. Bandosz, *J. Colloid Interface Sci.*, **210**, 367 (1999).
33. R. Hoyer, L. A. Kibler, and D. M. Kolb, *Electrochim. Acta*, **49**, 63 (2003).
34. T. J. Schmidt, N. M. Markovic, V. Stamenkovic, P. N. Ross, G. A. Attard, and D. J. Watson, *Langmuir*, **18**, 6969 (2002).
35. M. Arenz, V. Stamenkovic, T. J. Schmidt, K. Wandelt, P. N. Ross, and N. M. Markovic, *Surf. Sci.*, **523**, 199 (2003).
36. L. A. Kibler, M. Kleinert, R. Randler, and D. M. Kolb, *Surf. Sci.*, **443**, 19 (1999).
37. I. A. Pasti and S. V. Mentus, *Electrochim. Acta*, **55**, 1995 (2010).
38. N. Massoni, A. Beaumont-Martinent, and J. Y. Laurent, *J. Power Sources*, **166**, 68 (2007).
39. B. Scharifker and G. Hills, *Electrochim. Acta*, **28**, 879 (1983).
40. S. R. Brankovic, N. Dimitrov, and K. Sieradzki, *Electrochem. Solid-State Lett.*, **2**, 443 (1999).
41. H. Naohara, S. Ye, and K. Uosaki, *Colloid Surf. A: Physicochem. Eng. Aspects*, **154**, 201 (1999).
42. G. Jerkiewicz, *Electrocatal.*, **1**, 179 (2010).
43. Sasaki, H. Naohara, Y. Cai, Y. M. Choi, P. Liu, M. B. Vukmirovic, J. X. Wang, and R. R. Adzic, *Angew. Chem. Int. Ed.*, **49**, 8602 (2010).
44. J. Zhang, M. B. Vukmirovic, Y. Xu, M. Mavrikakis, and R. R. Adzic, *Angew. Chem. Int. Ed.*, **44**, 2132 (2005).
45. K. Sasaki, J. X. Wang, H. Naohara, N. Marinkovic, K. More, H. Inada, and R. R. Adzic, *Electrochim. Acta*, **55**, 2645 (2010).
46. M. Weyland, *Top. Catal.*, **21**, 175 (2002).
47. C. Thambidurai, Y. G. Kim, N. Jayaraju, V. Venkatasamy, and J. L. Stickney, *J. Electrochem. Soc.*, **156**, D261 (2009).
48. Y. Kim, Y. G. Kim, and J. L. Stickney, *J. Electrochem. Soc.*, **154**, D260 (2007).
49. F. Mrozek, Y. Xie, and M. J. Weaver, *Anal. Chem.*, **73**, 5953 (2001).